Journal of Advanced Research 28 (2021) 17–26

Contents lists available at ScienceDirect

Journal of Advanced Research

journal homepage: www.elsevier.com/locate/jare

Influence of occupant collision state parameters on the lumbar spinal injury during frontal crash

S. Sivasankari, Venkatesh Balasubramanian *

RBG Labs, Department of Engineering Design, IIT Madras, Chennai 600036, India

GRAPHICAL ABSTRACT

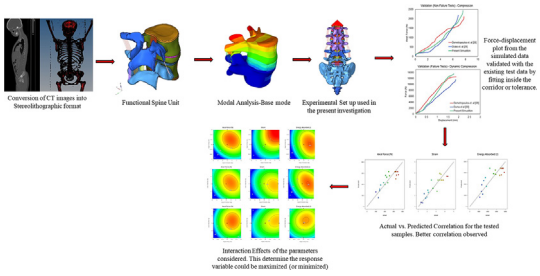

ARTICLE INFO

Article history:
Received 10 March 2020
Revised 25 May 2020
Accepted 10 June 2020
Available online 17 June 2020

Keywords:
Lumbar spinal injury
Response surface methodology
ANOVA
Height of drop
Seating posture angle
Mass of the Torso

ABSTRACT

Introduction: Developed a detailed finite element model of spine and validated with the experimental or cadaveric tests to gain insight on occupant safety.
Objectives: This study evaluates the influence of occupant collision state parameters such as height of the drop, occupant seating posture (occupant posture angle) and mass of the upper body on the risk of lumbar spinal injury during a frontal crash.
Methods: This parametric evaluation utilizing response surface methodology (RSM) performed. ANOVA was used to test the significance of parameters.
Results: Higher axial force of 3547 N is observed with higher dropping distance of 1500 mm. Similarly, higher strain and energy absorption were observed for the same dropping condition respectively.
Conclusion: The result shows that all the factors considered in the experiment contribute to the risk of spinal lumbar injury during the frontal crash. Among all, height of the drop and the occupant posture angle are the most significant parameters in determining the lumbar spinal injury of occupant. It is observed that the injury criteria are directly proportional to the posture angle of the seat and height of drop.

Introduction

The increasing trend in the lumbar injury during vehicle crash is highly alarming, as no crash testing regulation has not included the spinal injury measurement process (e.g. United States New Car Assessment Program (US-NCAP), Federal Motor Vehicle Safety Standard (FMVSS)208, and Insurance Institute for Highway Safety (IIHS)). This is due to the fact that the current Anthropomorphic Test Dummy (ATDs) dummies cannot precisely predict spine fracture risks [1]. Current ATDs were designed to help predict risk of injuries to the extreme edges and the upper body like chest, neck, head. Their assumed spine representation are not actual indicative of human anatomy and it lacks consideration for validation towards biomechanical impact response of any human/cadaver. Therefore, loads derived from the lumbar spine should be captured in the impact test, as it improves the capability to reflect the legit injury risk in the event of frontal crashes [2].

Peer review under responsibility of Cairo University.
* Corresponding author.
E-mail address: chanakya@iitm.ac.in (V. Balasubramanian).

https://doi.org/10.1016/j.jare.2020.06.010
2090-1232/

A widening trend of lumbar fractures was found in the frontal crashes from 1986 to 2008 of vehicle model year still after with continuous improvement in vehicle designs every year [3]. After the 2000, in late-model vehicles lumbar spine fractures occurred more than twice when compared to the 1990s vehicle models predominately with compression. In frontal crashes, the same study also investigated that five times more likely to have a major lumbar spine compression fracture is for belted occupants. From the similar research, it is stated that, lumbar burst fractures typically require an axial compressive load and have been known to occur during a non-horizontal crash event that involve high vertical components of loading [4]. Research from the German crash database [5] shows 15 percent of MAIS 2+ accidents involved lumbar spine injury.

High-energy axial compression is the key mechanism for lumbar fracture even with inclusion or exclusion of flexion in the biomechanical view of injury [6,7,8,9,10]. Earlier studies also shown that the loading due to axial compression by impact to the pelvis may occur during the event of speed bump ride in rear side of a bus, or combat incidents including the ejection of pilot seats and the smashing of underbody [11,12,13]. Furthermore, needs more clarity on mechanism as how an axial loading in frontal crashes will work on the lumbar spine of a fastened driver/passenger. In earlier times cadaver experiment by [14] reproduced the axial force occurred during frontal crashes along the lumbar spine transferred potentially from the seat pan, but at that time no further details can be given. The initial study [15] meant that 3 point fastened passenger still protected from lumbar fractures. It is mainly due to the pre-flexed lumbar spine for occupant pelvis with the lap belt in submarining. It is further hypothesized that in modern vehicle the axial force experienced in buttocks can contribute to spinal fracture especially burst fracture [16] due to the bucket seat of a belted occupant. The middle spine may be upright "suddenly and forcibly" as the shoulder belt holds the torso during a frontal crash [17]. Keeping all these in observance, this research focused on a parametric simulation using statistical analysis [17,18]. From the published information [19,20], understood that the lumbar spinal injury was focused on axial compression force by varying the height of drops. Very few investigations [20,21,22] have been conducted so far on lumbar spinal injury studies based on the various parameters like the velocity of drop and torso mass. However, none of the previously mentioned studies focused their efforts on the seating posture angle with this combinational study. Compression related lumbar fractures are occurring in frontal impacts and yet the mechanism of injury is not defined. Hence, the present study aimed to evaluate the effect of height of the drop, mass of the torso and seat posture angle on the characterization of lumbar injury criteria.

Experimental work

Data acquisition & image processing

A total of five people participated in the research study. The Apollo Research Center has collected the computed tomography data for the participants in A.E.R.B (Atomic Energy Regulatory Board, India) approved facilities. All the subjects were given a detailed explanation of the experiment, and their consent was taken in accordance with the standard guidelines. All participants were considered to be normal healthy working adults (mean age ± Standard deviation: 35.2 ± 3.12; mean weight of 67.5 Kg; mean height ± standard deviation 161.4 cm ± 7.5 cm). The medical reports was investigated before screening for degenerative and the pre-trauma diseases. X-rays were obtained with the Lumbar spinal column, all directions (lateral, anterior and posterior). Further, Positron Emission Tomography scans (PET) focusses on the biologic activity (Siemens Positron Emission Tomography CT Scanner & Siemens Healthineers, India) and axial computed tomography (CT) scans (Siemens CT Scanner - SOMATOM Definition Flash & Siemens Healthineers, India) gives anatomic information as slices of transverse plane and 2 mm intervals along the sagittal plane for reconstructions. Standard medical procedures were followed as per the guidelines of the Scan Centre, Apollo Research Center, India.

OsiriX, a software used for image processing, steadfast to the DICOM image format (with .dcm extension) files produced by imaging modalities (MRI, CT, PET, PET-CT, SPECT-CT, Ultrasounds) is used to read and process images for multiple operations. The .dcm format is the compatibility mode for files to be processed and the extracted data at 1250 threshold combined to sequence the slices of the computed tomography data as stereo-lithographic formatted data for further analysis using the CAD and FE software. Before converting the formatted data into FE, the model requires enhanced volumization of the CT data. The model further scaled and repaired with respect to the models available in the online depository [23]. Then the files are generated and formatted in *.stl file, an intermediate between the CT data and FE data can avail maximum feature in the converted stereo-lithographic files.

Volume generation and segmentation are carried out using HYPERMESH software, completely user-controlled methods which allow complete custom segmentation and volume generation. The insulation of each bone and disc into a separate collector makes operation simple. An additional benefit is the independence of assigning properties of the material to the isolated bones. Static structural anthropometry data from standard percentile male and female populations were referred to direct the process during the isolation process. The skeletal measurements were determined using static (structural) anthropometry. For optimal data retention several iterations of this task were performed. The lumbar five vertebra was segmented and grouped to a collector, and likewise the lumbar four vertebrae were segmented and organized into another collector. In the generated mesh discontinuity requires more steps to patch the surfaces and then generate a new volume. Intervertebral disc was modelled with the surfaces projected between the two end plates of the adjacent vertebra. The two vertebrae and one-inter vertebral disks produced combine as the Functional Spine Unit (FSU), the smallest part of the spine that can reflect all the main biomechanical characteristics of the whole spine. Its mechanical behaviors as a subsystem are characterized by the physical properties of the vertebrae, intervertebral disks and connecting ligaments. The seven ligaments are the flavum, intertransverse, inter-spinous, supraspinous, capsular, longitudinal anterior, and posterior ligaments. Fig. 1 showed the phases of data acquisition and image processing.

The intended material properties for analysis of the FSU were utilized for simulation purposes shown in Table 1. The classifications mentioned in Table 1 were incorporated to create an anatomically detailed 3D FE model with enhanced extracted features. The Finite element analysis was performed using commercially available software called Ls-Dyna.

In the developed model, the intervertebral disc was modeled as nucleus, annulus, and collagenous fibers. In order to represent the cortical bone, a layer of shell elements was added with 1 mm thick. Cortical bone was represented by element thickness of 1 mm. Modeled the ligaments as beam inserted in the assembly, wherever required as per the detailed anatomical and scan information. Intervertebral discs were modeled as solid elements. Articulations of the bones is defined using tie contacts for simulation between adjacent endplates. No muscles and its properties were not added in this investigation.

The developed lumbar model comprised of 375,111 elements and 92,497 nodes. Few bones are modeled as per

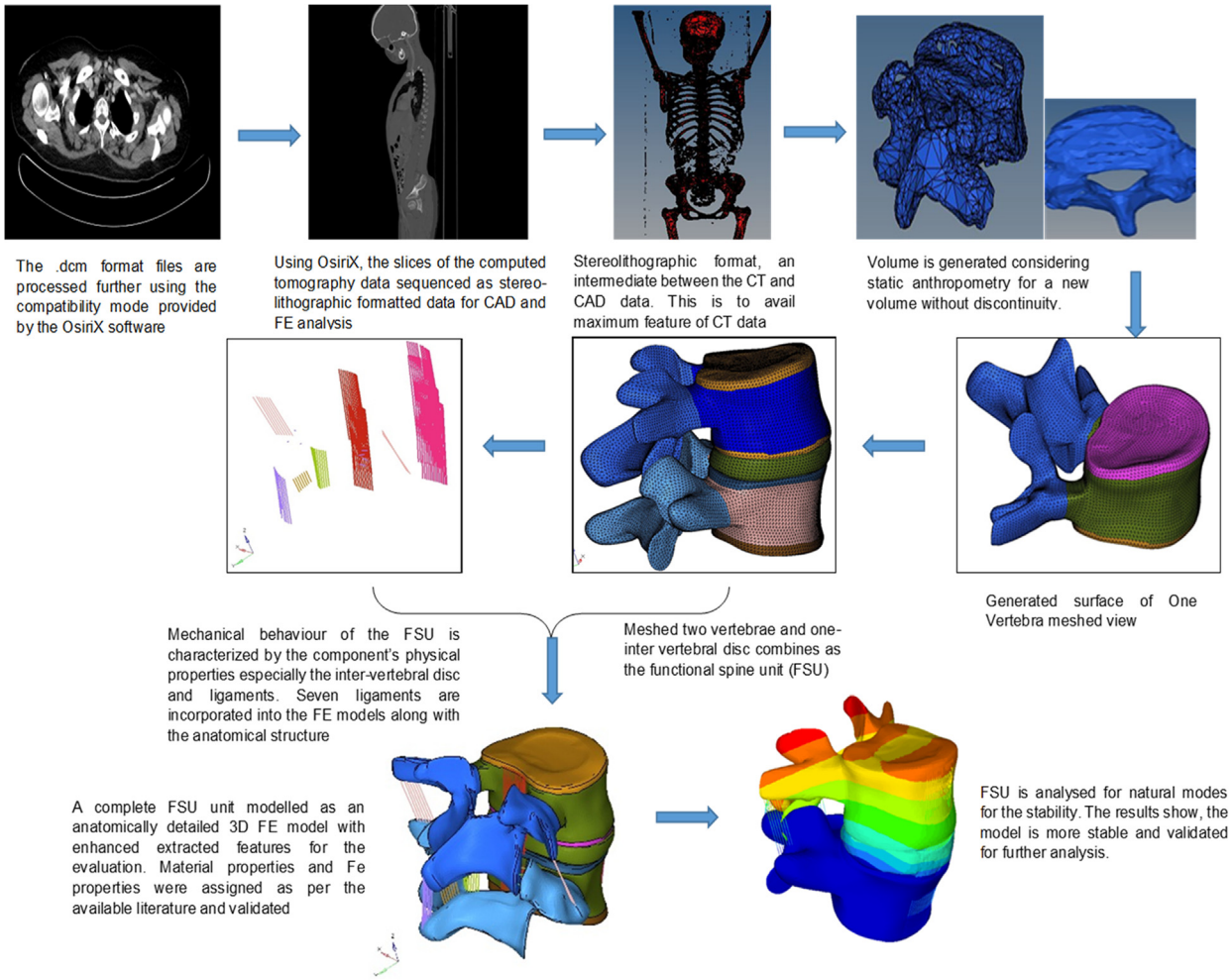

Fig. 1. Data acquisition and image processing techniques for model development. Existing literature cited in this research used the same methodology for model development. It was validated further with the cadaver tests cited in the next sequence.

Table 1
Material properties used in this current study.

Segments	Density (t/mm^3)	E (MPa)/K (N/mm)	Poisson ratio	A* (MPa)	B* (MPa)	N	C	PSFAIL	SIGMAX (MPa)	Stiffness of Ligaments (N/mm)					
										T12-L1	L1-L2	L2-L3	L3-L4	L4-L5	L5-S1
Cortical bone	1.81E−09	11,750	0.3	107	99	0.12	1	9.39E−03	160	–	–	–	–	–	–
Cancellous bone	1.80E−10	260	0.26	1.70	20	1	1	1.32E−02	1.99	–	–	–	–	–	–
Endplate vertebra	1.06E−09	9460	0.3	5.65	99	1	3	1.90E−02	7.15	–	–	–	–	–	–
Endplate disc	1.20E−09	10	0.3							–	–	–	–	–	–
Disc annulus	1.20E−09	0.49		0.24	−0.06					–	–	–	–	–	–
Disc nucleus	1.00E−09	0.50		0.64	−0.16					–	–	–	–	–	–
Fiber	1.20E−09	Curves								–	–	–	–	–	–
Anterior longitudinal ligament	1.00E−09									32.9	32.4	20.8	39.5	40.5	32.9
Posterior longitudinal ligament	1.00E−09									10	17.1	36.6	10.6	25.8	10
Ligamentum Flavum	1.00E−09									24.2	23	25.1	34.5	27.2	24.2
Facet Capsulary Ligament	1.00E−09									31.7	42.5	33.9	32.3	30.6	31.7
Inter Spinous ligament	1.00E−09									12.1	10	9.6	18.1	8.7	12.1
Supra Spinous ligament	1.00E−09									15.1	23	24.8	34.8	18	15.1
Inter-transverse ligament	1.00E−09									15.1	23	24.8	34.8	18	15.1

* In LS_DYNA material keywords, the strain energy density of MAT_MOONEY-RIVLIN_RUBBER is defined as a function of constant *A*, constant *B*, and Poisson ratio [32].

few published information [23,24]. In Ls-Dyna, the Mat_Simplified_Johnson_Cook material model is used for the cancellous and cortical bones. Plastic strain of 1.3% and 0.94% used, respectively. Similarly, Mat_Mooney_Rivlin_Rubber is used for modeling the nucleus and annulus. Its shear modulus constants A, B.are 0.65 MPa, −0.15 MPa and 0.25 MPa, −0.05 MPa respectively. Both the top and bottom endplates were modeled with Mat_Simplified_Johnson_Cook elastic material [25].

Ligaments were considered with elastic and linear beams. The stiffness of the ligaments was shown in Table 1 were based on a previous study [26,27,28]. For model validation, responses are modified using material characteristics of ligaments and bones to co-relate experimental validations.

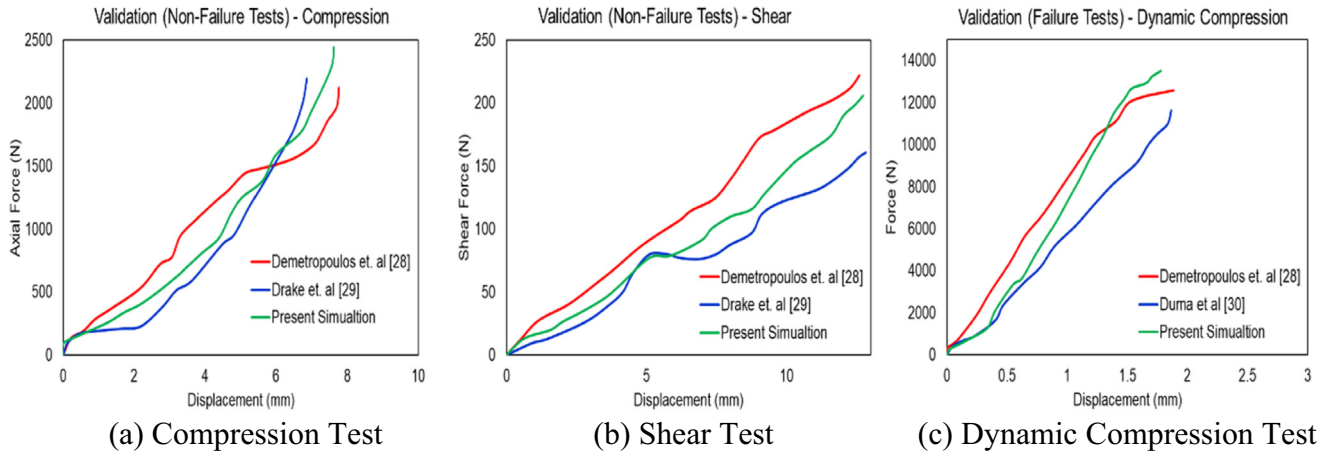

Fig. 2. Force-displacement curves in each loading condition for the modified lumbar spine model for (a) Compression test, (b) Shear test and (c) Dynamic Compression test. [29,30,31].

Validation with non failure experimental tests

From the previous research [29] cadaver data was used to validate the developed model. Initial position consistency was adjusted [30] to evaluate compression and shear strength. The loads were simulated corresponding to the test environment. Input velocity of 150 mm/sec was given and the output maximum displacement was measured. Applied the same displacement for the simulated model having boundary condition of constraints at top of L1 and bottom of coccyx.

The load applied on the bottom fixture with the upper constrained fixture. This is to simulate the compression and shear conditions shown in Fig. 2(a) & (b). Force versus Displacement plotted for the adapted lumbar spine model at each loading conditions with measured force responses. The simulated results should be well within the tested or referred corridors.

Validation with failure experimental tests

Data from the previous studies using cadaver tests with tissue failure [31] were used to validate the present investigation model. The current model is developed as the same configurations used for the dynamic compression test. Fig. 2(c) shows the displacement curve for the same setup. In this present study, simulations are carried out by fixing upper plate to L1 top end plates and lower plate to inferior end of the model. An initial velocity was applied to the model. All dofs were constrained on both upper and lower plates. The load rate was 1.0 m/s for the simulations to be carried out. In these simulations, force and moment were calculated under different loadings. Force versus Displacement plot for the adapted lumbar spine model at each loading configurations fell within the tested corridor.

Drop test simulation

Drop tests or drop tower tests are used to reproduce the impact during vertical loading, as component level or whole-body cadaver tests. This test is quite reliable with realistic loading and boundary conditions. This test is more capable of correlating the metrics with injury tolerance in the associated loading environment (i.e., Spine acceleration of lumbar from the base).

The test set up consists of a tower to vary the height and connected to a rail for guiding using linear bearings, and the bottom shape material can modulate the deceleration pulse. The same testing is replicate using FE simulations. The test comprises of the specimen to be mounted. It is raised to a specific required height and released. The generated gravity accelerates the setup towards the downward direction and gets impact by a specialized material [32] at the bottom of the tower shown in Fig. 3.

The displacement of the model is maintained using initial height, and with the material property of the profile shaped material. Any maximum accelerations can be achieved in simulation. However, in the test set up, maximum accelerations should be 65 G or with 2,500 G/s rate. In the current model, the torso mass is placed over the L1 at its center of gravity. The mass can be differed to represent specific torso mass or can retain constant for all specimens tested under a given standard. The components of the spine can be evaluated for compression. The load application can be moved in other way as mass is attached to the top portion based on the area of interests or

Different types of testing procedures are made available for the current model. The model is made enough to replicate real-world injuries for deriving the human tolerance and its injury mechanism and assessing biomechanical properties by means of forces and risk curves using this experimental setup.

Generally, the component level testing consists of isolated components of vertebral bodies tested to study the material response of the specific vertebral bodies to quantify the structural. Fig. 3 shows the testing of lumbar, which replicates the general drop tower test procedure. The tests are carried from quasi-static to

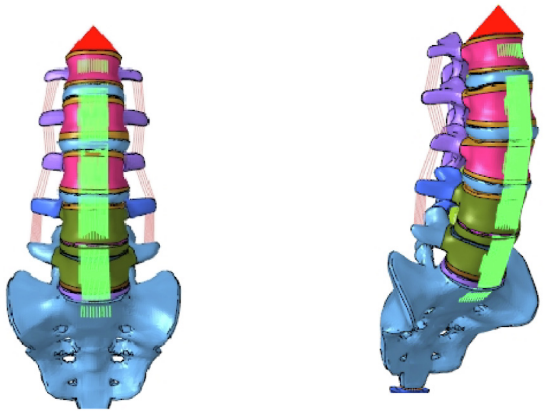

Fig. 3. Experimental Set up Used in the present investigation. This is the initial posture of the lumbar spine developed for the test simulation. MAT20 rigid elements [32] were used with the center of mass constraint along the translational direction for the stability of the model after impact.

Table 2
Ranges of factors considered for the present investigation.

Factor	Name	Units	Minimum	Maximum	Coded Low	Coded High	Mean	Std. Dev.
S_p	Occupant posture angle	deg	90.00	120.00	−1 ↔ 96.00	+1 ↔ 114.00	105.00	7.60
H_d	Height of Drop	mm	500.00	1500.00	−1 ↔ 700.00	+1 ↔ 1300.00	1000.00	253.40
M_t	Torso mass	kg	15.00	35.00	−1 ↔ 19.00	+1 ↔ 31.00	25.00	5.07

dynamic rates. In the present simulation, the axial force, strain and energy absorbed were measured. This can be used to understand the fracture in physiological level-by-level segmental kinematics with force output of the lumbar column using a drop tower apparatus during the application of dynamic axial load.

Finding the range of test parameters

Referring the literatures [33,34,35,36,37,38,39,40], the prevailing causes are recognized causes that have a greater influence on lumbar spinal damage during a frontal collision. We are I drop height, (ii) sitting angle posture, and (iii) upper body mass. Large numbers of trial experiments were simulated using the drop test to determine the feasible test conditions. Are derived the following inferences.

- If the height of the drop was lesser than 500 mm, the energy absorption is reduced to the lower level. No considerable effect on the lumbar spinal is observed. This is classified under group A [33].
- If the height of drop was greater than 500 mm, the energy absorption is higher and unpredicted to classify under group B. May cause damage to the system extensively [34].
- If the seating posture angle was lesser than 90 degrees, the comfortability is reduced in the occupant. Moreover, no seat is defined any of the vehicles with lesser 90 degrees inclination from the horizontal platform [35].
- If the seating posture angle was greater than 120 degrees, comfortability is not eased. However, still 120 degrees is feasible after the existence of autonomous vehicles [36].
- If the magnitude of masses was lesser than 15 kg, the energy absorption is reduced to the lower level. During lower energy tests, the specimen did not sustain injuries which allowed further evaluation for sub-failure and failure tests of biomechanical data from the same specimen [37,38].
- If the magnitude of masses was greater than 35 kg, the energy absorption is unpredictable. However, the mass calculation from 15 kg to 35 kg was based on a mid-size male occupant torso according to the automotive specifications [39,40].

Experimental matrix development

To utilize the extensive range of three factors and to optimize the number of experiments using central composite rotatable design matrix. The experimental settings for the factors of the reaction were considered at 0 for the mid and (±1) stages. The design was spread to a 1.68 ± α (axial point). For the error calculation and individual runs for each variable, the center values for variables were performed minimum six times; twenty runs were conducted in a completely random arrangement. The concept consists of the 2^3 cube's eight corner points, six axial points and six center points. Axial points having $\alpha = 1.682$ for $\alpha = 8^{(1/4)}$. In this investigation, matrix composed of 20 sets of implicit conditions (including six corner points, six center points and a full replication of three 8-point factorials) was selected. Table 2 represents the range of considered factors. Sampling and simulation using Design Expert v12. 20 sets of predicted and experimental values utilized for the experiments shown in Table 3. ±1.682 as lower and upper level, for ease of documenting and analyzing experimental data. Using experimental factors and ranges the following relationship can be established;

$$\alpha_i = 1.682[2\alpha - (\alpha_{max} - \alpha_{min})]/[(\alpha_{max} - \alpha_{min})] \quad (1)$$

where αi is the intended code values of a variable α, where α is any values of the variable from αmin to αmax; the upper level of the variable is αmax and the lower level is αmin.

Table 3
20 sets of coded and actual values used to conduct the experiments.

Runs	Occupant posture angle (S_p) deg	Height of Drop (H_d) mm	Torso mass (M_t) kg	Axial Force N	Strain –	Energy absorbed J
1	96	700	19	1285	1.48	11204.7
2	114	700	19	2344	2.65	38802.2
3	96	1300	19	2033	1.97	13068.3
4	114	1300	19	2544	3.56	28453.9
5	96	700	31	1423	1.3	18,765
6	114	700	31	1877	1.66	29,344
7	96	1300	31	2222	2.07	17460.6
8	114	1300	31	2098	3.43	26,734
9	90	1000	25	1433	1.33	14,567
10	120	1000	25	3333	4.33	28,765
11	105	500	25	999	1.83	15,664
12	105	1500	25	3547	4.22	35,432
13	105	1000	15	1546	2.13	13,456
14	105	1000	35	3245	3.11	33,585
15	105	1000	25	2444	2.47	22,536
16	105	1000	25	3456	3.82	36,574
17	105	1000	25	3144	3.56	34,524
18	105	1000	25	3222	3.22	35,678
19	105	1000	25	3254	3.67	37,543
20	105	1000	25	3277	3.37	37,543

Table 4
ANOVA for the Quadratic terms used in the present investigation.

Source	Sum of Squares			df	Mean Square			F-value			p-value			VIF
	Axial Force	Strain	Energy		AxialForce	Strain	Energy	Axial Force	Strain	Energy	Axial Force	Strain	Energy	
Model	9.819E +06	15.24	1.271E +09	9	1.091E +06	1.69	1.412E +08	3.33	5.24	2.70	0.037*	0.008*	0.069*	
S_p Occupant posture angle	1.894E +06	6.63	5.520E +08	1	1.894E +06	6.63	5.520E +08	5.77	20.53	10.56	0.038*	0.001*	0.008*	1.0000
H_d Height of Drop	2.849E +06	4.63	3.115E +07	1	2.849E +06	4.63	3.115E +07	8.69	14.34	0.5957	0.014*	0.003*	0.045*	1.0000
M_t Torso mass	3.720E +05	0.013	8.691E +07	1	3.720E +05	0.0139	8.691E +07	1.13	0.04	1.66	0.031*	0.084	0.026*	1.0000
S_p H_d	1.585E +05	0.25	2.284E +07	1	1.585E +05	0.2521	2.284E +07	0.4832	0.78	0.4368	0.042*	0.037*	0.012*	1.0000
S_p M_t	1.922E +05	0.13	6.688E +07	1	1.922E +05	0.1352	6.688E +07	0.5860	0.42	1.28	0.461	0.531	0.028*	1.0000
H_d M_t	648.00	0.16	2.611E +06	1	648.00	0.1625	2.611E +06	0.0020	0.50	0.0499	0.026*	0.049*	0.011*	1.0000
S_p2	1.595E +06	1.26	2.731E +08	1	1.595E +06	1.26	2.731E +08	4.86	3.92	5.22	0.052	0.761	0.045*	1.02
H_d2	1.992E +06	0.74	1.275E +08	1	1.992E +06	0.7426	1.275E +08	6.07	2.30	2.44	0.033*	0.160	0.149	1.02
M_t2	1.553E +06	1.98	1.967E +08	1	1.553E +06	1.98	1.967E +08	4.73	6.14	3.76	0.054	0.032*	0.031*	1.02
Residual	3.280E +06	3.23	5.229E +08	10	3.280E +05	0.3229	5.229E +07							
Lack of Fit	2.657E +06	2.07	3.566E +08	5	5.314E +05	0.4139	7.133E +07	4.27	1.79	2.15	0.068	0.270	0.211	
Pure Error	6.225E +05	1.16	1.662E +08	5	1.245E +05	0.2318	3.324E +07							
Cor Total	1.310E +07	18.47	1.794E +09	19										

* Marked values shows ($p < 0.05$), the terms are significant.

Results & discussion

Developed an empirical relationship

For this study, the Response Surface Methodology (RSM) was implemented because of its benefits to determine the interactions effects between measured parameters [41,42].

In the present investigation, a quadratic model was established to correlate the parameters with lumbar spinal injury. The response (adsorbed by axial force, strain and energy) is a function of occupant seat posture (S_p), drop height (H_d) and torso mass (M_t), and expressed as

$$Lumbarspinalinjury = f(S_p, H_d, M_t). \quad (2)$$

Design of experiments were used to study the combinational effects of the factors considered, using design expert software. The analytical relationship essentially comprises principal and interaction effects are specified below:

$$\lambda = \theta_o + \sum \theta_i x_i + \sum \theta_{ii} x_i^2 + \sum \theta_{ij} x_i x_j. \quad (3)$$

For the 3 factors, the chosen polynomial can be stated as

$$\begin{aligned} \text{Lumbar spinal injury} = \{&\theta_0 + \theta_1(S_p) + \theta_2(H_d) + \theta_3(M_t) \\ &+ \theta_{11}\left(S_p^2\right) + \theta_{22}\left(H_d^2\right) + \theta_{33}\left(M_t^2\right) \\ &+ \theta_{12}(S_p \cdot H_d) + \theta_{13}(S_p \cdot M_t) + \theta_{23}(H_d \cdot M_t)\} \end{aligned} \quad (4)$$

where θ_0 is the average of responses (Lumbar Spinal Injury), and θ_1, θ_2, $\theta_3 \ldots \theta_{11}$, θ_{12}, $\theta_{13} \ldots \theta_{22}$, θ_{23}, θ_{33} are the coefficients with respect to major and interrelated parameters, can be expressed as follows;

$$\beta_i = \Sigma(\eta i, \Phi i) \quad (5)$$

where "i" ranges from 1 to n, where and "n" is total f combinations, ηi is the relevant implicit value, Φi is the relevant response (lumbar spinal injury) acquired from the experiment.

All the coefficients were calculated using a rotatable design matrix for the central composite including the statistical software package for the Design Expert. The final relationship was established for axial force, strain and energy absorbed after assessing the relevant coefficients with 95 percent confidence. The empirical relationship developed to predict the lumbar spinal injury are as follows.

$$\begin{aligned} \text{Axial Force} = &(-87.15S_p^2 - 135.26H_d^2 - 115.24M_t^2) \\ &+ (2.98H_dM_{tt} - 48.21S_p \cdot H_d - 64.29S_pM_t) \\ &+ (121.87S_p + 153.26H_d + 55.24M) \\ &+ 1241.55 \end{aligned} \quad (6)$$

$$\begin{aligned} \text{Strain} = &(0.303S_p^2 - 0.2301H_d^2 - 0.3759M_t^2) + (0.1425H_dM_t \\ &+ 0.1775S_pH_d - 0.1300S_pM_t) + (0.6993S_p \\ &+ 0.5845H_d + 0.0320M_t) + 3.37 \end{aligned} \quad (7)$$

$$\begin{aligned} \text{Energy Absorbed} = &(-54.47S_p^2 - 0.0034H_d^2 - 101.04M_t^2) \\ &+ (-0.625S_pH_d - 53.541S_pM_t \\ &+ 0.318H_dM_t) + (1411.91S_p \\ &+ 129.816H_d + 10927.18M_t) + 95334.1 \end{aligned} \quad (8)$$

The coded equations can make predictions about the response of each factor for all levels. +1 and −1 are the high and the low factor levels. The coded equation identifies the correlation between the factors by comparing the factor coefficients.

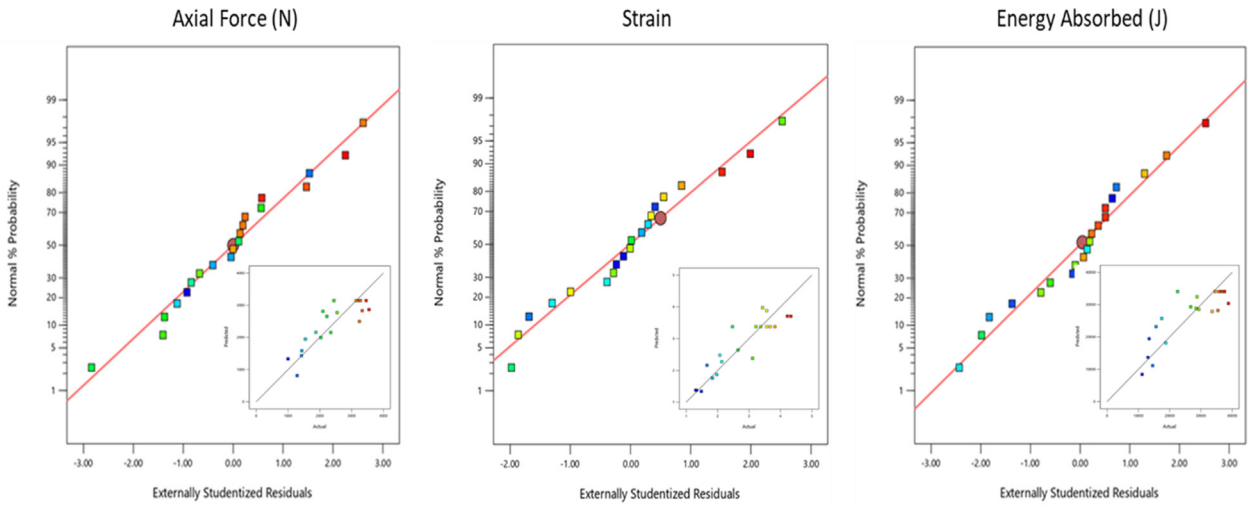

Fig. 4. Normal Probability plots for the tested samples to analyse the data distribution. The present data sets are normally distributed. Embedded plot is the correlation between experimental and the predicted samples. Predicted value are based on a semi-empirical model (Correlation) that was developed for the responses and factors. From the investigation, it uses the correlation to set new responses at a certain confidence level set for the factors.

$$\text{Axial Force} = (-337.19S_p^2 - 376.79H_d^2 - 332.69M_t^2) + (-140.75S_p \cdot H_d - 155.00S_pM_t + 9.00H_dM_t) + (373.77S_p + 458.46H_d + 165.66M_t) + 3145.72 \quad (9)$$

$$\text{Strain} = (-0.004S_p^2 - 0.002H_d^2 - 0.015M_t^2) + (-0.001S_pH_d - 0.002S_pM_t + 0.001H_dM_t) + (0.085S_p + 0.002H_d + 0.701M_t) + 54.26 \quad (10)$$

$$\text{Energy Absorbed} = (-4412.00S_p^2 - 3014.48H_d^2 - 101.04M_t^2) + (-1689.68S_pH_d - 2891.33S_pM_t + 571.28H_dM_t) + (6381.06S_p + 1515.81H_d + 2532.01M_t) + 34056.35 \quad (11)$$

The actual equations can make predictions about the response of each factor for all levels and not the correlation. All original units were considered. For correlation, the intercepts deviated from center space with scaled coefficients.

Determining the significant factors (ANOVA)

The factors available in the present investigation were coded. Type III – Partial is used for the equation of sum of squares. Table 4 shows the ANOVA for the quadratic terms used in the present investigation. The two-way ANOVA used the mean difference between groups divided into two variables and compared it. The main objective of a two-way ANOVA is to figure out if the dependent variables communicate with each other. It also lets you know if the effect of any of your independent variables on the dependent variable is the same for all other variables [18].

Model F-values are 3.33, 5.34 and 2.70 for the axial force, strain and energy respectively. This indicates the model is significant. Due to noise, only 3.74 percent, 0.81 percent and 6.88 percent are probable to appear. P value ($p < 0.05$) indicates the significance of the established model. Hence, S_p, H_d, M_t, S_pH_d, H_dM_t & H_d^2 are significant factors for axial force. Similarly, S_p, H_d, S_p H_d, H_dM_t & M_t^2 are significant factors for strain. Furthermore, S_p, H_d, M_t, S_pH_d, H_dM_t, S_pM_t, S_p^2 & M_t^2 are significant factors for energy.

F-value of 4.27, 1.79 and 2.15 means that the absence of fit is not important compared to the pure error as its ($p > 0.05$). There are 15.60%, 27.00% and 22.10% chances that Lack of Fit F-value is high, due to noise. Non-significant lack of fit is good.

Adequate Precision ratio above 4 is desirable and signal to noise ratio can be calculated from its precision in the testing. The ratio of the current model was 5.757, 6.550 and 5.009 for force, strain and energy absorption. As the values are above 4 it indicates an adequate signal and the design space can be navigated for this model. The Predicted and Adjusted R^2 of strain are 0.0594 and 0.6678 with the gap more than 0.2 requires confirmation runs for relevance in the model data.

Estimation of the significance of the coefficient

The coefficient estimate represents the predicted variation in response of the factor value keeping all other factors remains constant. The average of all responses can be approximated to the intercept in the orthogonal design. Coefficients were calculated based on the average adjustments of the factor considered. The orthogonal factors recommend the VIF equal to one. Multicollinearity observed with the VIFs greater than 1 [43]. Severity in correlation among the factors found with the higher values of VIFs. Tolerance limit is applied to VIFs < 10 considered to be a rule and the results were shown in Table 4

To evaluate if the model follows the given assumptions in the analysis, certain criteria to be obtained. Fig. 4 shows the normal probability plots examined how closely the data points follow the fitted distribution line, also assessed the probability plot. The determined theoretical distribution is a good fit, as the data points fall similar pattern along the straight line. In general, the points in the normal probability plot follow the line well. The normal distribution seems to be a good fit for the data without skewness, as there is no long or short tail observed,

Also, the normal probability plot confirms the assumptions, or the experimentations are met. If the assumptions were unsatisfied, unfit in the data is observed and caution should be exercised when the results are interpreted.

The assumed residuals have to be randomly distributed with constant variance. By using the residuals versus fits plot, the assumption was verified. Ideal condition is, the data points should fall randomly on either side's datum. No recognizable patterns may

be observed. The points were scattered and appears to be fitted. No variations and no outliers are obvious. The fitness of predicted versus experimental data were embedded in the respective normal probability plots shown in Fig. 4.

It shows a good fit, as the points lie close to the fitted line with narrow confidence bands. Points furthest from the mean on either side of the plots attracts the fitted line towards data points. Outliers are the scattered points found vertically on both sided of the fitted line. These outliers can affect the model undesirably in terms of fitness. The predicted versus experimental plot shown in Fig. 4 also represents a pictorial view of the results derived using analysis of variance, gives better understanding that the derivation from a hypothesis analysis. This shows that confidence interval surrounds the model line depicts the hypothesis test contains all factors are zero excluding the intercepts. If hypothesis test is found significant, then, there is no interval of confidence containing horizontal zero model line.

Individuals & interaction effects of parameters

Perturbation plot shows the comparison between all factors at a selected point in the considered design space. The perturbation plot for the axial force, strain and energy absorbed are shown in Fig. 5. The axial force and strain response were drawn by changing only one factor over its range while the other factors were held constant. The plot demonstrates the effect of all factors at a central point in the design space. Not all factors indicated a positive effect on the lumbar spinal injury. The relatively flat line of torso mass shows lower effect of this factor on the lumbar spinal injury in the design space. From the plot, the steep curvature in parameters demonstrated the response of axial force and strain were very rapid to these factors. This shows, all the parameters or factors considered are having significant effect on the lumbar spinal injury

Furthermore, the models show good fittings, the response values are sufficiently explained by the regression equation. The interaction between the independent variables were demonstrated using the response surface curves which determines the optimal value of each independent variable for the maximum response. The 2D contour plots were provided as graphical representations of the regression equations shown in Fig. 6.

Fig. 6a shows the response surface function developed by the model for the height of drop and occupant posture angle. The occupant posture angle demonstrated quadratic effects on the response. With the increase in occupant posture angle, axial force increases. It is also observed that, the height of drop increases till 1300 mm. Further increase in the axial force is with respect to the occupant posture angle. Similarly, Fig. 6b shows the linear effect of the parameters on the response. With the increase in axial force and occupant posture angle, the strain is increased. The same is clearly observed in the ANOVA table (p: value). Fig. 6c shows the interaction between the occupant posture angle and the height of drop on energy absorbed. More energy is absorbed with the increase in occupant posture angle than the height of drop. The response surface is more curved because the quadratic terms contain in the models are statistically significant.

An increase in the axial force, strain and energy absorbed were significantly with the increases in occupant posture angle and torso mass shown in Fig. 6(d), (e) and (f). However, axial force and strain no longer increase when the independent variables exceeded certain values. An occupant posture angle and torso mass were not statistically significant in affecting the axial force and strain, but it had a significant (P less than 0.01) effect on energy absorption.

Similarly, the height of the drop and torso mass demonstrated quadratic effects on the responses shown in Fig. 6(g), (h) and (i) The results of the effects of the height of drop and torso mass on the axial force are shown in Fig. 5(g). Both the parameters are dependent and displayed a quadratic effect on the axial force between 60 and 70% of the axial force. Similarly, strain increases

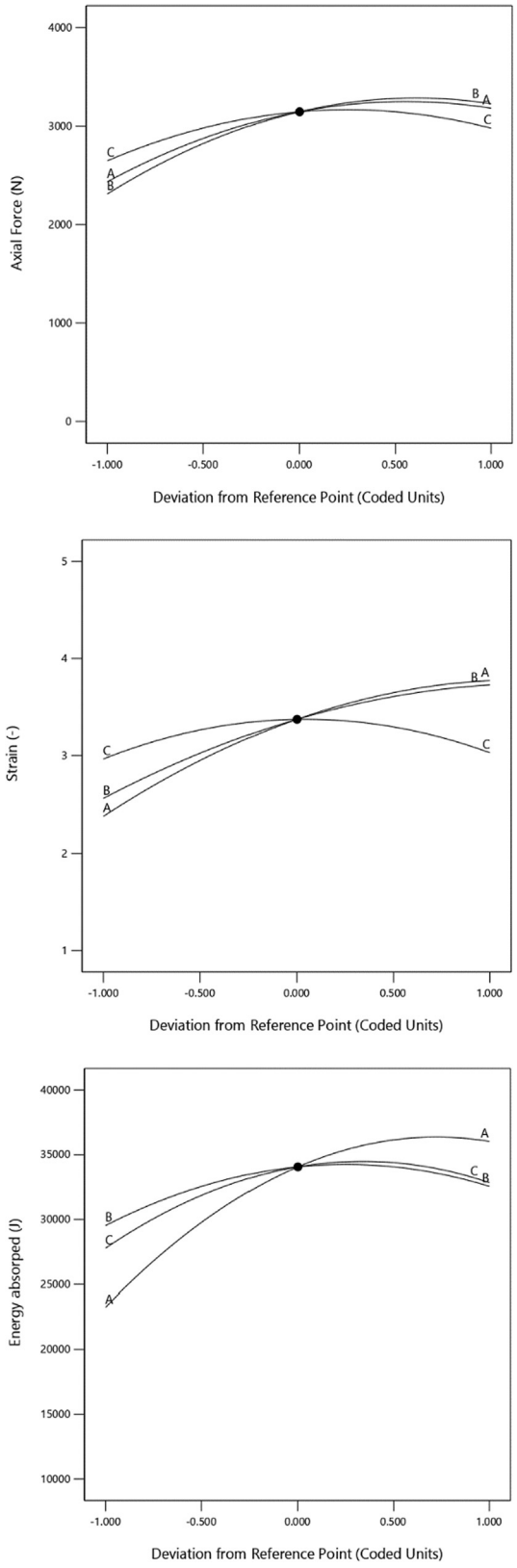

Fig. 5. Perturbation Plot of the samples. Perturbation plot showing the effect of factors (process variables).

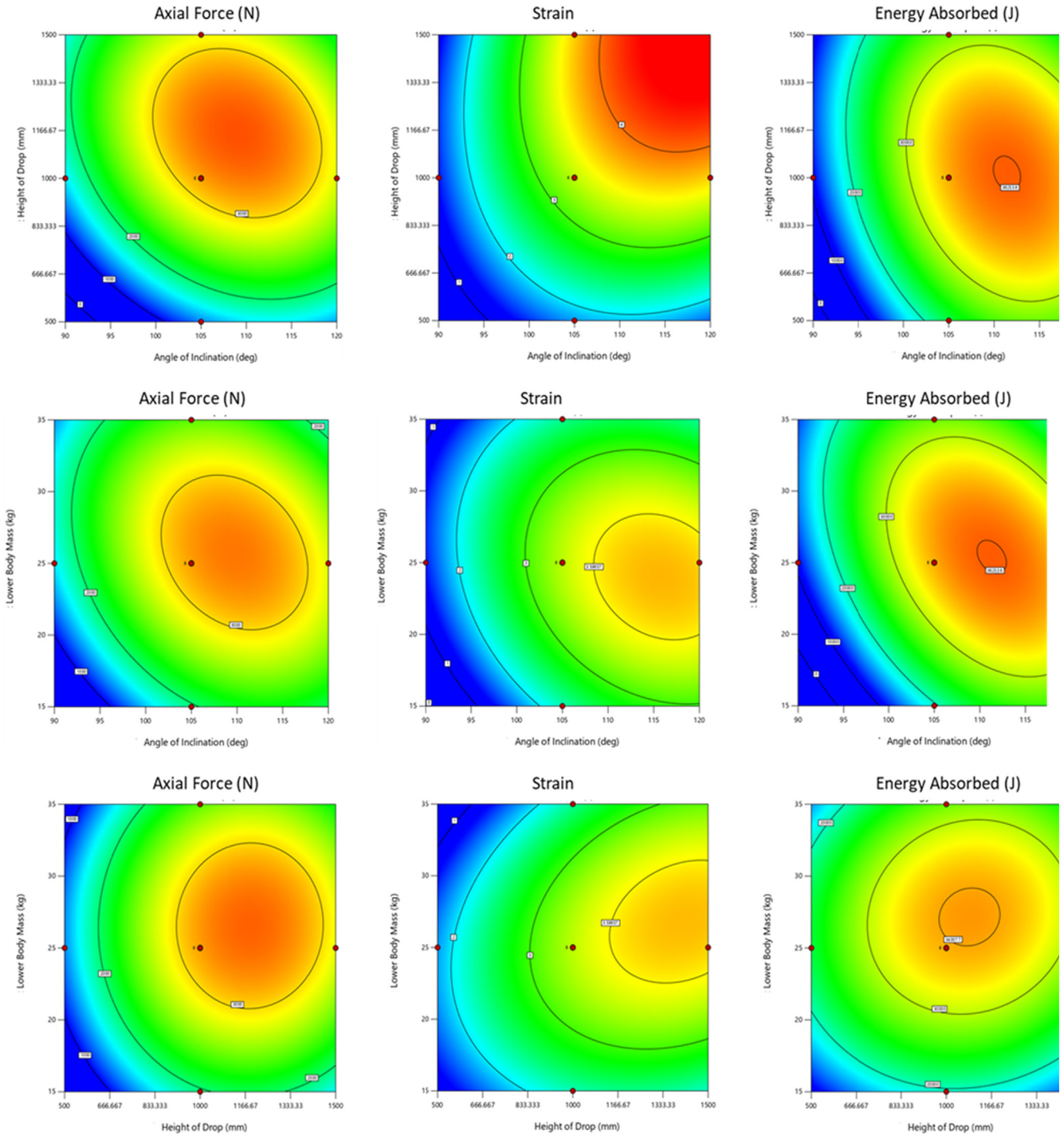

Fig. 6. Interaction Effects of the parameters considered. These plots shown are in determining settings that will maximize (or minimize) the response variable. It can also be helpful in determining settings that result in the response variable hitting a pre-determined target value.

with the increase in height of drop, when solvent composition was fixed. Energy absorption increased gradually and reached the highest value when the height of drop is around 1300 mm.

Conclusions

1. An empirical relationship was developed to predict the axial force, strain and energy absorbed by the lumbar spine during the vertical impact of the vehicle crash using drop testing with a 95% confidence level.
2. With the increase in the height of drop and occupant posture angle, the responses were increased. However, the effects on the torso in lesser compared to other parameters.
3. It is observed that interaction between the height of drop and occupant posture angle is quite significant.
4. This study can provide fundamental information and valuable insight into the automotive crash and impacts for the better design for the safety of occupants.

Compliance with Ethics Requirements

All procedures followed were in accordance with the ethical standards of the responsible committee on human experimentation (institutional and national) and with the Helsinki Declaration of 1975, as revised in 2008 (5). Informed consent was obtained from all patients for being included in the study.

The emphasis of this study was in performing CAE studies in-silico. Geometric structures used in the study was using retrospective CTs from five subjects of healthy individual. This study owing to the nature of it being CAE work, didn't have any ethical committee approvals. Hence it was exempted.

Funding

This research did not receive any specific grant from funding agencies in the public, commercial, or not-for-profit sectors.

Declaration of Competing Interest

The authors declare that they have no known competing financial interests or personal relationships that could have appeared to influence the work reported in this paper.

References

[1] Federal Register:: Federal Motor Vehicle Safety Standards; Occupant Crash Protection n.d. https://www.federalregister.gov/documents/2019/09/27/2019-20644/federal-motor-vehicle-safety-standards-occupant-crash-protection (accessed February 13, 2020).
[2] Nahum AM, Melvin JW. Accidental injury: biomechanics and prevention. Springer Science & Business Media; 2012.
[3] Pintar FA, Yoganandan N, Maiman DJ, Scarboro M, Rudd RW. Thoracolumbar spine fractures in frontal impact crashes. Ann Adv Automot Med 2012;56:277.
[4] Kaufman RP, Ching RP, Willis MM, Mack CD, Gross JA, Bulger EM. Burst fractures of the lumbar spine in frontal crashes. Accid Anal Prev 2013;59:153–63.
[5] Adolph T, Wisch M, Eggers A, Johannsen H, Cuerden R, Carroll J, et al. Analyses of thoracic and lumbar spine injuries in frontal impacts. Proc. IRCOBI Conf. Biomech. Impacts; 2013.
[6] Richards D, Carhart M, Raasch C, Pierce J, Steffey D, Ostarello A. Incidence of thoracic and lumbar spine injuries for restrained occupants in frontal collisions. Annu Proc/Assoc Adv Automot Med 2006;50:125.
[7] Ivancic PC. Hybrid cadaveric/surrogate model of thoracolumbar spine injury due to simulated fall from height. Accid Anal Prev 2013;59:185–91.
[8] Munjin MA, Zamorano JJ, Marré B, Ilabaca F, Ballesteros V, Martinez C, et al. Speed hump spine fractures: injury mechanism and case series. Clin Spine Surg 2011;24:386–9.
[9] Kikuike K, Uemura S, Miyamoto K, Horiya Y, Shimizu K. Upper lumbar burst fracture due to recreational high jumping into a river: report of five cases. Arch Orthop Trauma Surg 2009;129:87.
[10] Gertzbein SD, Khoury D, Bullington A, St John TA, Larson AI. Thoracic and lumbar fractures associated with skiing and snowboarding injuries according to the AO Comprehensive Classification. Am J Sports Med 2012;40:1750–4.
[11] Du C, Mo Z, Tian S, Wang L, Fan J, Liu S, et al. Biomechanical investigation of thoracolumbar spine in different postures during ejection using a combined finite element and multi-body approach. Int j Numer Method Biomed Eng 2014;30:1121–31.
[12] Ragel BT, Allred CD, Brevard S, Davis RT, Frank EH. Fractures of the thoracolumbar spine sustained by soldiers in vehicles attacked by improvised explosive devices. Spine (Phila Pa 1976) 2009;34:2400–5.
[13] Wang H, Zhang Y, Xiang Q, Wang X, Li C, Xiong H, et al. Epidemiology of traumatic spinal fractures: experience from medical university–affiliated hospitals in Chongqing, China, 2001–2010. J Neurosurg Spine 2012;17:459–68.
[14] Begeman PC, King AI, Prasad P. Spinal loads resulting from-Gx acceleration; 1973.
[15] Huelke DF, Mackay GM, Morris A. Vertebral column injuries and lap-shoulder belts. J Trauma Acute Care Surg 1995;38:547–56.
[16] Hu J, Klinich KD, Manary MA, Flannagan CAC, Narayanaswamy P, Reed MP, et al. Does unbelted safety requirement affect protection for belted occupants?. Traffic Inj Prev 2017;18:S85–95.
[17] Kleijnen JPC. Response surface methodology for constrained simulation optimization: An overview. Simul Model Pract Theory 2008;16:50–64.
[18] Qasim A, Nisar S, Shah A, Khalid MS, Sheikh MA. Optimization of process parameters for machining of AISI-1045 steel using Taguchi design and ANOVA. Simul Model Pract Theory 2015;59:36–51.
[19] Ball ST, Vaccaro AR, Albert TJ, Cotler JM. Injuries of the thoracolumbar spine associated with restraint use in head-on motor vehicle accidents. Clin Spine Surg 2000;13:297–304.
[20] Jacobs RR, Asher MA, Snider RK. Thoracolumbar spinal injuries. A comparative study of recumbent and operative treatment in 100 patients. Spine (Phila Pa 1976) 1980;5:463–77.
[21] Demetropoulos CK, Palepu V, Goel VK. Biomechanics of Spinal Trauma; 2012.
[22] Ferguson RL, Allen JBL. A mechanistic classification of thoracolumbar spine fractures. Clin Orthop Relat Res 1984:77–88.
[23] Mitsuhashi N, Fujieda K, Tamura T, Kawamoto S, Takagi T, Okubo K. BodyParts3D: 3D structure database for anatomical concepts. Nucleic Acids Res 2009;37:D782–5.
[24] El-Rich M, Arnoux P-J, Wagnac E, Brunet C, Aubin C-E. Finite element investigation of the loading rate effect on the spinal load-sharing changes under impact conditions. J Biomech 2009;42:1252–62.
[25] Wagnac E, Arnoux P-J, Garo A, Aubin C-E. Finite element analysis of the influence of loading rate on a model of the full lumbar spine under dynamic loading conditions. Med Biol Eng Comput 2012;50:903–15.
[26] Pintar FA, Yoganandan N, Myers T, Elhagediab A, Sances Jr A. Biomechanical properties of human lumbar spine ligaments. J Biomech 1992;25:1351–6.
[27] Shirazi-Adl A. Biomechanics of the lumbar spine in sagittal/lateral moments. Spine (Phila Pa 1976) 1994;19:2407–14.
[28] Brickley-Parsons D, Glimcher MJ. Is the chemistry of collagen in intervertebral discs an expression of Wolff's Law? A study of the human lumbar spine. Spine (Phila Pa 1976) 1984;9:148–63.
[29] Demetropoulos CK, Yang KH, Grimm MJ, Khalil TB, King AI. Mechanical properties of the cadaveric and Hybrid III lumbar spines. SAE Trans 1998:2862–71.
[30] Drake JDM, Callaghan JP. Do flexion/extension postures affect the in vivo passive lumbar spine response to applied axial twist moments?. Clin Biomech 2008;23:510–9.
[31] Duma SM, Kemper AR, McNeely DM, Brolinson PG, Matsuoka F. Biomechanical response of the lumbar spine in dynamic compression. Biomed Sci Instrum 2006;42:476–81.
[32] Gladman B, others. LS-Dyna Keyword Users' Manual. Livermore Softw Corp Calif; 2007.
[33] Yoganandan N, Cusick JF, Pintar FA, Droese K, Reinartz J. Cyclic compression-flexion loading of the human lumbar spine. Spine (Phila Pa 1976) 1994;19:784–90.
[34] Yoganandan N, Larson SJ, Gallagher M, Pintar FA, Reinartz J. Droese K. Correlation of microtrauma in the lumbar spine with intraosseous pressures. Spine (Phila Pa 1976) 1994;19:435–40.
[35] Pintar FA, Yoganandan N, Moore J. Spine and pelvis fractures in axial Z-acceleration. Proc. 40th Int. Work. Hum. Subj. Biomech. Res.; 2012.
[36] Yoganandan N, Pintar F, Sances Jr A, Maiman D, Myklebust J, Harris G, et al. Biomechanical investigations of the human thoracolumbar spine. SAE Trans 1988:676–84.
[37] Zheng J, Tang L, Hu J. A numerical investigation of risk factors affecting lumbar spine injuries using a detailed lumbar model. Appl Bionics Biomech 2018. https://doi.org/10.1155/2018/8626102.
[38] Yoganandan N, Pintar FA, Gennarelli TA, Seipel R, Marks R. Biomechanical tolerance of calcaneal fractures. Annu Proc/Assoc Adv Automot Med 1999;43:345.
[39] Yoganandan N, Maiman DJ, Pintar FA, Bennett GJ, Larson SJ. Biomechanical effects of laminectomy on thoracic spine stability. Neurosurgery 1993;32:604–10.
[40] Yoganandan N, Sances JA, Pintar F, Maiman DJ, Reinartz J, Cusick JF, et al. Injury biomechanics of the human cervical column. Spine (Phila Pa 1976) 1990;15:1031–9.
[41] Venugopal S, Mahendran G. Development of an empirical relationship to predict the joint tensile strength and joint shear strength of diffusion bonded AA6082 aluminium alloy. Int J Mater Prod Technol 2019;58:257–74.
[42] Tang L, Zheng J, Hu J. A numerical investigation of factors affecting lumbar spine injuries in frontal crashes. Accid Anal Prev 2020;136:105400.
[43] James G, Witten D, Hastie T, Tibshirani R. An introduction to statistical learning; 2013.